https://doi.org/10.1016/j.ymssp.2022.109508

A Hierarchical Deep Convolutional Regression Framework with Sensor Network Fail-safe Adaptation for Acoustic-emission-based Structural Health Monitoring

Shifeng GUO[a,b], Hao DING[a,c], Yehai LI[a,b,*], Haowen FENG[a,b], Xinhong XIONG[c], Zhongqing SU[d], and Wei FENG[b,*]

[a]Shenzhen Key Laboratory of Smart Sensing and Intelligent Systems

Shenzhen Institute of Advanced Technology, Chinese Academy of Sciences, Shenzhen 518055, P.R. China

[b]Guangdong Provincial Key Lab of Robotics and Intelligent System

Shenzhen Institute of Advanced Technology, Chinese Academy of Sciences, Shenzhen 518055, P.R. China

[c]School of Transportation and Logistics Engineering

Wuhan University of Technology, Wuhan 430070, P.R. China

[d]Department of Mechanical Engineering

The Hong Kong Polytechnic University, Hung Hom, Kowloon 999077, Hong Kong SAR

Submitted to *Mechanical Systems and Signal Processing*

(submitted on 19th October 2021, revised and re-submitted on 31st May 2022)

* To whom correspondence should be addressed. Email: yh.li@siat.ac.cn
* To whom correspondence should be addressed. Email: wei.feng@siat.ac.cn

Abstract

Lamb wave-based signals from sparse-distributed sensors are complicated and difficult to process for structural health monitoring (SHM), not only due to their dispersive and multi-mode nature, but also due to the increasing complexity of materials and structures. Deep learning (DL) has attracted huge attention to help solve physical problems with a high level of automation and accuracy. However, its reliability and robustness are still questioned when performing the case-by-case model trained by inadequate datasets for practical scenarios, where many variables exist. In this study, a hierarchical deep convolutional regression framework is proposed to solve the impact source localization problem by acoustic emission signals. One-dimensional (1D) network is used due to its capability to process fast with raw time-series data. The window length of input data and the target of output results are discussed to improve the over-fitting issue. The sensor network fail-safe mechanism is designed via generalizing the model to handle abnormal situations with random faulty channels. Data augmentation and transfer learning techniques are utilized to train the fail-safe model without the need for additional experimental data. Pristine case and multiple random-faulty-channel cases are used to test and validate the adaptation performance of the fail-safe model. The whole framework combines both pristine and fail-safe models to achieve high accuracy of impact localization results of both a simple homogeneous plate and a complex inhomogeneous plate with geometric features. The proposed DL framework of greatly improved reliability and robustness, also short processing time, is well suitable for real-time and *in-situ* SHM applications.

***Keywords*:** structural health monitoring; deep learning; convolutional neural network; acoustic emission; Lamb wave; impact localization

1. Introduction

Structural health monitoring (SHM) is a real-time and *in-situ* damage identification technology of engineering structures for condition-based maintenance. This technology involves a variety of techniques to be implemented, among which Lamb wave exhibits a great potential for plate-like structures due to its advantages as long-distance propagation, easy actuation and reception, and sensitivity to defects [1]. Data acquisition of Lamb wave-based SHM relies on sparse-distributed sensors to capture wave response over a large scanning area, along with the dispersive and multi-modal nature of Lamb wave, which complicate the signals and make the analysis and interpretation of them a daunting task for engineers. Conventional physics-based methods extract damage-related features (*e.g.,* mode conversion, wave scattering, and attenuation) by studying the Lamb wave propagation behaviors [2, 3] and the interaction with defects [4-6]. However, the ever-increasing degree of complexity with the systems, from both materials (*e.g.,* anisotropic composites and multi-layer heterogeneity) and structures (*e.g.,* with stiffeners, joints, and holes), intensifies the need for more sophisticated signal processing methods.

The development of statistics-based methods like data-driven machine learning (ML) offers alternative solutions for interpreting signals [7-9], with no need for a priori knowledge of structural/material properties, in hope of achieving autonomous solutions with minimal requirement and dependence on human knowledge and experience. Algorithms like support vector machine (SVM) [10] and artificial neural network (ANN) [11-13] have been widely exploited for Lamb wave-based SHM over the last two decades. However, these ML algorithms usually require extensive data pre-processing (such as de-noising and feature extraction) which are often time-consuming and relying on domain expertise, therefore not suitable for real-time and automated damage detection. In recent years, with the rapid

development of computational capability, deep learning (DL) has emerged as a novel powerful approach not only in fields like computer vision and language processing, but also in industry diagnosis applications coping with a variety of non-destructive testing (NDT) methods [14], for example, crack detection by vision [15], welding detection using X-Ray images [16] and inspecting damaged composite structures using infrared (IR) images [17]. Lamb wave-based SHM also has the potential to benefit from DL due to its intricate behaviors [18] (*e.g.,* damping, dispersion, reverberation, distortion, and multimodal characteristics). The high-level damage-related features hidden in the complex Lamb wave response, if recognized, can greatly improve the evaluation of the structure state. One of the major advantages of DL over other ML algorithms is that it can auto-extract high-level features, without the need for data pre-processing and human hand-picking, therefore leading to high accuracy of damage identification and increased automation level, albeit at the cost of large datasets and high computational capability.

Taking acoustic emission (AE) as an example, a typical kind of passive SHM for crack extension and impact detection which is also the focus in this study, the instant broadband excitation makes the waveforms highly dispersive and complicated. Physics-based diagnosis methods utilize only simplified features, including triangulation via time of arrival [19], delta-T mapping [20], and reciprocal time-reversal [21, 22]. These techniques have intuitive and straightforward physical significance and their performance of source localization results would be limited by parameters in physical models, for example, the accuracy of pre-known wave velocity and calculated arrival time in triangulation methods. Moreover, a minimum number of sensors is required to perform. It is almost impossible to localize AE sources via a single sensor unless leveraging edge reflections by complicated physical knowledge and tomography algorithms [23, 24]. On the other hand, DL could automatically

extract high-level features and perform AE source localization via a single sensor [25]. It was also shown that convolutional neural network (CNN), one of the most widely used DL algorithms, outperformed not only physics-based methods [26], but also classical ML algorithms as ANN [27] and SVM [26] in AE source diagnosis. More sophisticatedly, Zargar and Yuan [28] designed a hybrid CNN-RNN (recurrent neural network) framework to auto-extract spatial-temporal features from full wavefields for impact monitoring.

However, like other ML algorithms, DL models are susceptible to over-fitting, *i.e.,* only perform well on the training data but poorly on unseen data. In SHM applications, due to the numerous variables in real conditions, the input data for training is inherently not *i.i.d*. and would become unseen data with a little change (from environment, instruments, stochasticity of dynamical systems, *etc.*). Over-fitting means that the DL model fails to learn the physical problem or insufficiently generalizes to practical scenarios. This raises two major issues which are highly concerned in the engineering world: reliability and robustness. For real-time *in-situ* SHM, false or missing alerts would highly jeopardize the practical value and hence of little tolerance. The prediction accuracy of DL for SHM is tendentiously very high in most reported work. However, if there exists the possibility of imbalanced data or leakage of testing data into training datasets, its performance in real scenarios may become a "Garbage in - Garbage out" process. For example, since the experimental data of Lamb wave-based SHM is difficult to obtain for a large amount, analytical or numerical simulation results were widely used as input data to train DL models, either solely [29, 30] or together with a small portion of experiment data [31, 32]. Physical models in the analytical or numerical simulation are highly idealized that results may match well with the experimental data for the first-arrived waves [29], but deviate as the time increasing while involving complex physical phenomena as mode conversion, dispersion, scattering, reflection, *etc.*

[33]. Thus, the reliability of such DL models trained by simulation results is uncertain in real scenarios. There are several methods to reduce over-fitting by modifying the training network, such as weight regularization and dropout [32, 34]. However, the DL model works as a "black box" and it is difficult to control target-relevant features to be extracted. Therefore, researchers tried to use a priori physical knowledge to bias the learned features not to be misrepresentative [28, 33, 35]. A typical example is to superimpose artificial random noise to simulation results to augment input data, and DL models can learn to focus on low-frequency features rather than superfluous high-frequency features in real data [29, 33]. Another example is to time-reverse the extracted wave-propagating features from time-series data to focus the outputted source locations [28].

On the other hand, a robust DL algorithm must be generalized enough to avoid the "Garbage in - Garbage out" process with variation in the input model in similar cases. Generally, a DL model is specifically tailored to learn how to solve a particular problem, *i.e.*, if test data are not obtained for exactly the same model, they will be treated as bad input and the outcome would be a poor output. For industry applications as NDT, if the inspected structures are of different geometry, dimensions, or materials from the training structure, or operated under different conditions, the used DL model must be retrained with new training data and labels recollected from every new situation, which is significantly expensive and often impossible. *In-situ* Lamb wave-based SHM, in particular, relies on fixed sensors on structures to transmit diagnostic signals [36], hence the varied properties of sensor networks in real physical situations should be considered in the design of DL models and verification of prediction accuracy. Ewald et al. [30] discussed the accuracy of CNN-predicted damage locations with different sensor layouts by repeated training for each individual case. Liu et al. [37] investigated the influence of sensor number on predicted AE source location errors by a

101 regression neural network via also individual training processes. Zhang et al. [38] considered
102 the non-uniform bonding quality of sensors by data argumentation in training the CNN
103 model which could be used directly on a different plate. For impact detection by AE, each
104 impact is an independent event, the detection of which relies on one-shot measurement.
105 However, there is a high chance that one or several channels in the sensor network cannot
106 give correct responses at that moment, possibly due to failure, environment influences of
107 temperature and humidity, crosstalk from nearby electric devices, poor contact of wires,
108 electro-magnetic interference or others. These influences may be temporal but there is no
109 chance to detect again. Captured signals with one or several faulty channels would usually
110 be regarded as erroneous data and be removed from input dataset for training and test [37].
111 Such trained model would cause missing or false alerts in real SHM applications with
112 possible random-faulty-channel situations.
113
114 In this work, a hierarchical deep learning framework was proposed for AE source detection.
115 Impact simulated by ball drop was stochastic excitation resembling the reality that the
116 excited AE waveforms would not be the same even dropped at the same place due to slight
117 variations of impact angle, rotation of the ball in the air, imbalanced holder force, or
118 fluctuation of the base. Thus, there is little possibility of leaking testing data into training
119 datasets and the reliability and robustness of proposed methods can be tested and validated
120 by sufficient unseen data. Moreover, through a self-assembled automated impact stage, it
121 was convenient to obtain large enough datasets for DL, without concerning about the
122 reliability issue associated with adopting simulation results. The main body of the proposed
123 framework was a one-dimensional residual network (1D-ResNet) model. A regression layer
124 was implemented to acquire impact locations rather than zone-wise classification tasks in
125 many others' work of coarse resolution [27, 29, 39]. The over-fitting issue was also discussed

by quality control of the input and output with physical bias. Most importantly, the situations of random faulty channels were considered. The input multi-channel signals were firstly processed by a CNN model for fast binary classification to identify and isolate faulty channels. Data augmentation and transfer learning by inductive bias based on physical nature were implemented during the network training process, in order to generalize the model with adaptation to a bunch of random-faulty-channel cases. The proposed method was further verified on a complex inhomogeneous plate with geometric features. To the best of the authors' knowledge, it is the first time such a practical fail-safe mechanism being considered in developing DL-assisted SHM methods of high robustness and reliability.

2. Problem Descriptions

AE waves typically propagate as Lamb waves in thin-plate structures, which could induce challenge for feature extraction in physics-based source localization methods. Taking example for time-of-arrival (TOA) or time-difference-of-arrival (TDOA) based methods, to triangulate the source, the arrival time of wavefronts at each of the sensors needs to be estimated accurately, and also the group velocity of the corresponding wave mode. However, for low-velocity impact events, A_0 mode is dominant as compared to the S_0 mode with high amplitude in the low-frequency range but is also highly dispersive. As illustrated in **Figure 1**, different frequency components propagate with different group velocities, thus the wave energy would spread over time with the increase of the distance. Initial waveforms from impact location A would be elongated with distance, *i.e.* waveforms could be different when arriving at different sensors (S1 and S2). Conventional picker methods like threshold crossing would struggle with the accurate determination of arrival time and group velocity of dispersive wave modes even on a simple homogeneous plate, resulting in drastically decrease in the performance of source localization. Complicated signal processing methods

like wavelet transformation could be used but require expert knowledge [40]. Moreover, other interference could also affect the results, like attenuation, edge reflections, mode conversion, and plate echoes, which further complicate waveforms.

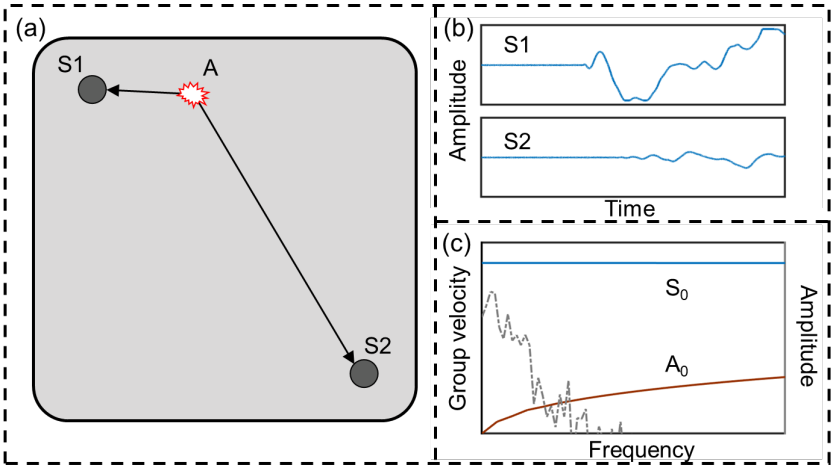

Figure 1. (a) Illustration of a simple homogeneous plate; (b) acquired AE signals of different propagation distances; (c) dispersion curves at the low-frequency range and the frequency bandwidth of AE signals.

Another important issue is related to the complex inhomogeneous structures with geometric features like stiffeners, bolts, and holes, which are common in engineering practice. The assumption of straight-line propagation is invalid. An example is shown in **Figure 2**, where the impact-generated wave at the center A can propagate in a straight line to some sensors (S2 and S3) but not to others (S1 and S4) due to the obstruction of internal cavities. Thus, the waveforms would be different even with the same distance between the source and the sensors.

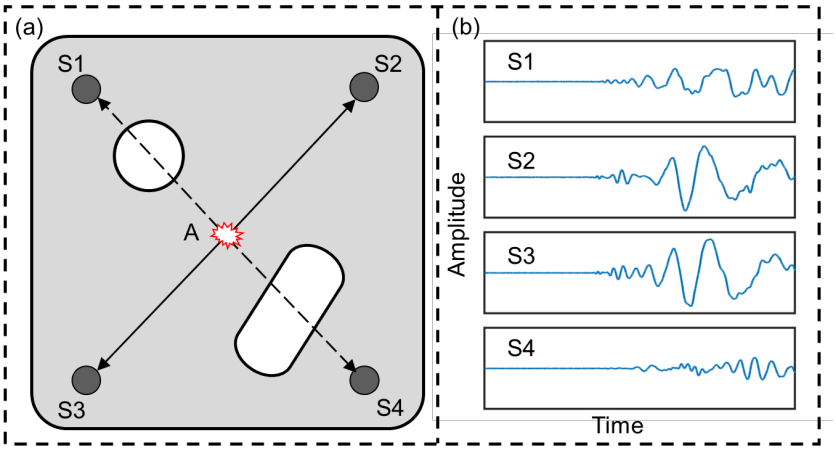

Figure 2. (a) Illustration of a complex inhomogeneous plate with two internal cavities; (b) acquired AE signals with the same straight distance.

DL algorithms have unique advantages as autonomous feature extraction and source localization. However, they are vulnerable to certain practical issues, like faulty signals due to environmental or electrical noise. The occurrence of faulty signals is generally stochastic in sensor channels and diversiform for each impact event. Even with only one faulty channel in the input space, the output could be adversely influenced. This work is focused on enhancing the robustness of DL models by considering fail-safe adaptation. A preliminary study will be implemented on a simple homogeneous plate first. Later a case study on a complex plate with two arbitrary cavities will be used to verify the effectiveness of the proposed method. The other complex inhomogeneities like varying thickness, reinforcement of different material compositions, and anisotropic composites will be left for future studies.

Although not the focus of this study, the optimal number of sensors is an interesting topic worthy to be mentioned. For physical-based methods, minimum requirement exists due to limited features used. For example, the TDOA-based methods require at least three sensors in isotropic and homogeneous plates with pre-known wave velocity [19]. On the other hand, DL-based methods have the potential to work with a single sensor [25], benefitting from the high-level implicit features auto-extracted from the whole signals with sufficient information rather than only TDOA of direct waves. Although few sensors are attractive from the point of view of cabling and costs, a certain degree of redundancy is necessary by considering system reliability against environmental noise, geometric scattering, material attenuation, *etc.* [41]. By increasing the number of sensors, the accuracy of source localization can be improved. Thus, there is no general solution, since each application has different constraints [42]. In this study, to fully investigate the fail-safe adaptation performance of the proposed method, a redundant network of eight sensors for a square-shaped plate was used, with diverse faulty-channel situations.

3. Proposed DL-assisted Impact Detection Method

3.1. Introduction to CNN

CNN is a feed-forward neural network based on convolution kernels to extract useful features, which can be categorized as 1D-CNN, 2D-CNN, and 3D-CNN by the type of input or dimensions of convolution direction. 1D-CNN is mostly used on series datasets to identify the local pattern within the one-dimensional window. It is generally used for analyzing signal data recorded by sensors, audio, *etc.* 2D-CNN is used on two-dimensional matrix datasets like images. 3D-CNN is the further extension of 2D-CNN with the input of three-dimensional volumetric data or a sequence of two-dimensional matrices (*e.g.* slices in a computer tomography scan, frames in a video) [43]. Since CNN has achieved great success in the computer vision field, researchers tried to transfer those 2D-CNN models to Lamb wave-based SHM. As the 2D-CNN kernel slides in two directions (length and width), certain transformation methods are required to convert time-series acoustic signals into 2D images (either in RGB or grey-scale format), for example through short-time Fourier transformation [29, 30, 33] and wavelet transformation [24, 44, 45] into time-frequency domain data. Although time-frequency data was proven to contain rich information for AE signals in physics-based methods [40, 46], the problem is that such transformation usually takes significant time, which is not suitable for real-time SHM. Another issue is that transform algorithms are highly dependent on the basis function and window size by human-picking, which weakens the automation advantage of DL algorithms. Moreover, the processing of 2D images is computationally costly and certain compression is necessary, which would result in loss of information about the high-level damage features hidden in the raw Lamb wave signals. This problem may not be important for object recognition in computer vision, but would get serious in the damage diagnosis field where time resolution is highly important for accurate results. Furthermore, some researchers tried to transfer pre-trained CNN models

from the computer vision field to acoustic-based damage diagnosis applications, to increase the training efficiency and mitigate the need for large training datasets [24, 28, 29, 47]. Although good results were achieved, controversies about the validation exist with concern about the fundamentally different physical meanings between optical images and acoustic waves [30]. 1D-CNN, on the other hand, has proven its ability to analyze discrete time-series data and identify local features within the selected window [31, 32, 38]. It allows raw signal input without extensive data pre-processing, and thus is suitable for real-time SHM. It also reduces the computational cost and minimizes the loss of information from the signal conversion. In a few studies, DL was used to process 3D wave data comprised of frames of wave propagation on a 2D plane along time [28, 48]. Such full wavefields can only be captured by scanning laser Doppler vibrometer, high-speed camera, or simulation, which are not applicable for SHM either in time consuming or measurement system. Therefore, 1D-CNN is worthy of exploiting for interpreting raw time-series acoustic signals in Lamb wave-based SHM.

Deep residual network (ResNet) is an improved CNN algorithm to handle the problems of gradient instability and network degradation when using deep networks to solve complex tasks [49]. It is characterized by a basic unit that may appear multiple times in the architecture which is called a residual block (ResBlock). Within each ResBlock, residual features are learned by introducing extra shortcut connections to skip over several layers. Considering the complexity of Lamb wave signals, the deep neural network is favored for feature extraction with a sufficient number of hidden layers. Thus, in this study, a one-dimensional residual network (1D-ResNet) model with multiple branches was proposed.

3.2. Architecture of the 1D-ResNet model

The proposed 1D-ResNet model is shown in **Figure 3**. There are six kinds of layers used,

which are convolutional (Conv) layer, batch normalization (BN) layer, rectified linear unit (ReLU), max-pooling (MaxPool) layer, average-pooling (AverPool) layer, and fully-connected (FC) layer. The roles played by these layers are feature extraction, accelerating training, nonlinear combination, features selection (both types of pooling layer), and regression, respectively. The time-series data of eight channels as input of the network is first reduced by a Conv layer with a kernel size of 7 and a stride of 2, then passed to a MaxPool layer with a pooling size of 3 and a stride of 2. These two layers are both used for dimensionality reduction. The reduced vectors are then inputted to three branches simultaneously. Each branch is composed of three sequential ResBlocks with increasing input channels from 64, 128 to 256. These ResBlocks are used to extract features such as the rising edge, falling edge, sharp change, gentle segment, and other features of the input signals. The difference among the three branches is the convolution kernel sizes in ResBlocks increasing from 3, 5 to 7. Within each ResBlock (illustrated in **Figure 3**), the feature extraction path consists of Conv layer, BN layer, and ReLU, with a shortcut connection path skipping directly from input to output. Outcomes of both paths are merged to be the output of the total block after being activated by

$$y = f(h(x) + F(x, W)), \quad \textbf{(1)}$$

where x is the input of this block, F stands for the transform of weight layers, and W is the weights used. $h(x)$ demonstrates the way of shortcut connection which is usually equal to x. f is the activation function of ReLU here.

After passing through multiple ResBlocks of multiple branches, the receptive fields of the features extracted in the original input signals are substantially increased. The obtained features from low level to high level can contribute synergistically to predicting results. At the end of the three branches, AverPool layers are used to reduce the dimensions of the

extracted features map, and then all extracted features are integrated into a large feature vector. The feature vector will be further regressed by two FC layers with a ReLU activation function between them.

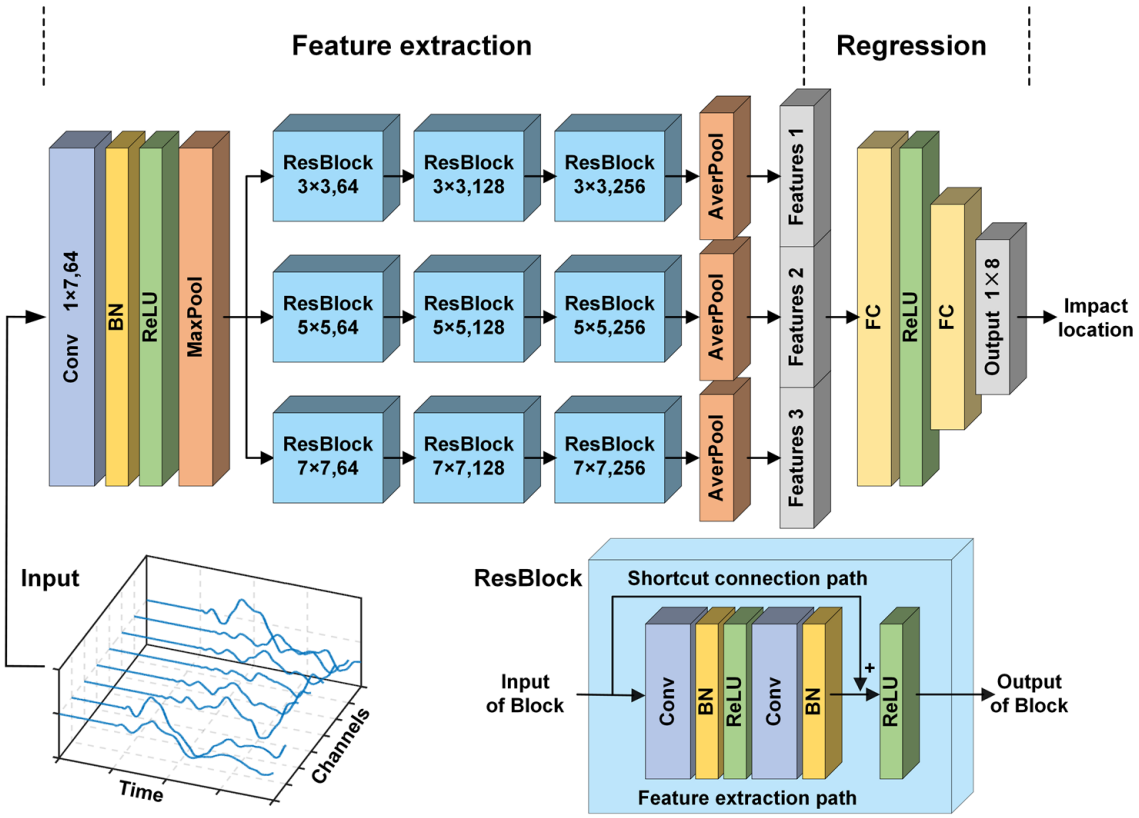

Figure 3. Architecture of the proposed 1D-ResNet model.

The output target of the network in this study is a 1×8 vector, corresponding to eight predicted distances from impact location to the positions of eight sensors. The reason is that AE signals from different sensors may not produce results of the same accuracy, considering the distance influence from the source to sensors. To mitigate the possibly-raised over-fitting issue, the targets of convergence are relaxed as eight individual source-to-sensor distance values. The results were compared with the common "End-to-End" output of a 1×2 vector as the predicted impact location in the form of x and y coordinates. Resembling the physics-based time-of-flight identification method that deals with ellipse-like or hyperbola-like damage loci [4], for each sensor a circle can be drawn as the locus of the source. Multiple loci lead to intersections. To achieve the final predicted results of impact locations, an intersection-clustering algorithm is proposed and detailed in **Table 1**. An example of three

sensors is shown in **Figure 4**. Firstly, six points are obtained from intersecting three circles of three sensors (for the non-intersecting cases, two closest points from the two circles are used instead). Then the center point is calculated and the farthest point is removed. After that, the new center point is calculated again. This is one-step clustering. After three times repeating the clustering step, the final predicted center result is obtained. In this study, eight sensors were used and thus 28 steps of clustering were required.

Table 1
Procedure of the proposed intersection-clustering method.

Input: M-number of sensors; P-positions of M sensors; D-outputted distances to M sensors.
Output: L-predicted impact location.
1. Plot M circles which use P_i as the center and D_i as the radius for i^{th} sensor;
2. Calculate all intersections of each pair of M circles, integrating a set $\boldsymbol{I}$ with a total number of $2C_M^2$;
3. Set k as the number of remaining intersections with an initial of $2C_M^2$;
4. **While** ($k > C_M^2$) **do**
5. Calculate the center of current intersections in $\boldsymbol{I}$ as point C;
6. Calculate the offset O from each intersection in $\boldsymbol{I}$ to C;
7. Remove the intersection with the largest O from $\boldsymbol{I}$, k −= 1;
8. Obtain C of the last $\boldsymbol{I}$, as L;
9. **return** L

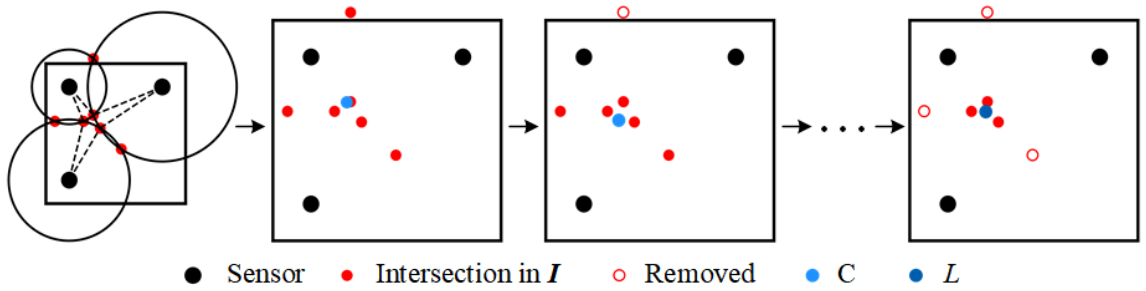

Figure 4. Example of the intersection-clustering procedure with three sensors.

3.3. Hierarchical framework with sensor network fail-safe adaptation

Based on the proposed 1D-ResNet and localization method, a hierarchical framework with generalized sensor network fail-safe adaptation is designed as shown in **Figure 5**. There are

two phases and three models in this framework. In the training phase, a 1D-ResNet model will be trained firstly with full-set data of all channels under pristine conditions (*i.e.,* no faulty channel in all input data). Then the pre-trained model is transferred to learn from a random-faulty-channel dataset for the fail-safe model. The sensor faulty situations are complicated and diversiform. It is impractical to obtain experimental data on all possible faulty cases. Thus in this study, the random-faulty-channel dataset is achieved by data augmentation from the original full-functioned-channel dataset. Deactivating λ channels by artificially setting the value as zero yields faulty-channel data with 8-λ good channels.

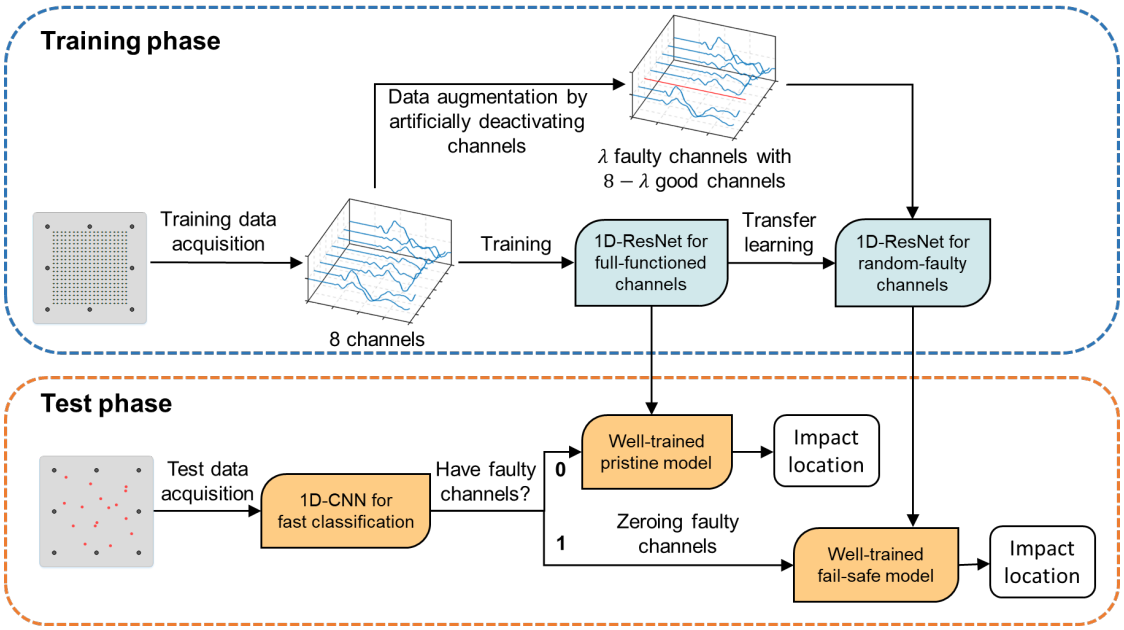

Figure 5. Schematic diagram of the proposed hierarchical framework.

In the test phase, the test data with unknown conditions are firstly processed by a 1D-CNN model for binary classification. The classification model has a simple structure comprised of two Conv layers, two ReLU layers, one MaxPool layer, and one AverPool layer for feature extraction. Then the extracted features go through one FC layer and one ReLU to perform feature linear and nonlinear transformations. Finally, a soft-max layer outputs two values between 0-1 for each channel, corresponding to the probability of good and faulty cases. For the case of all-good channels, the well-trained pristine model is used to predict. Otherwise, the faulty channels are identified and zeroed to uniform all kinds of faulty signal forms and

316 conform the input data to the fail-safe training data. Then the well-trained fail-safe model is
317 used to predict.
318
319 The training and testing were implemented in the PyTorch deep learning framework
320 (developed by the Facebook AI team) in a normal computer system with CPU of Intel Core
321 i7-9700, GPU of NVIDIA Quadro P2200 with 5 GB video memory, and RAM of 16 GB.
322 The API NVIDIA CUDA with version 10.2 was installed to accelerate the training process.
323 The Adam optimizer was used with a momentum of 0.9. The learning rate was set to be
324 0.002 as the initial value and exponentially decayed with training epochs. The training mini-
325 batch size was set to be 8.

326 **4. Preliminary Study on A Simple Homogeneous Plate**

327 *4.1. Experimental setup and dataset acquisition*

328 As shown in **Figure 6**, a 6061 aluminum plate with a size of 300×300 mm^2 and a thickness
329 of 2 mm was chosen as the study object. A sensor network comprising eight lead zirconate
330 titanate wafers (PZT, PSnN-5 from Yu Hai Electronic Ceramics) was pasted on the surface
331 by ethyl acrylate adhesive. Sensor location optimization was not concerned in this study.
332 Thus, the eight PZTs were deployed along the outer perimeter of the plate to inspect the area
333 within as the common way. The aluminum plate was suspended and fixed on the horizontal
334 test bench by clamps to avoid vibration interference. In order to obtain sufficient and
335 reproducible data for training and testing, a three-axis automated impact stage was designed
336 and assembled. The stage was controlled by a main unit of the stm32F407 chip with three
337 closed-loop motors for precise movement in the x-y plane and pre-set drop height. A
338 triggerable electromagnet unit was fixed on the slider. The impact was simulated by
339 dropping a ferromagnetic ball with a diameter of 7 mm and a mass of 14 g. This ball was

firmly attached to the electromagnet by electric charging. The unit stopped at every intersection of the training grid to perform a drop impact by discharging. The eight-channel data acquisition device (NI PXIe-5105) was used to capture AE signals from sensors synchronously at a sampling rate of 10 MSP/s. The acquisition length was set as 6144 sampling points (SPs) which equaled about 610 μs. Such window length was sufficient to record wave signals for all impact cases.

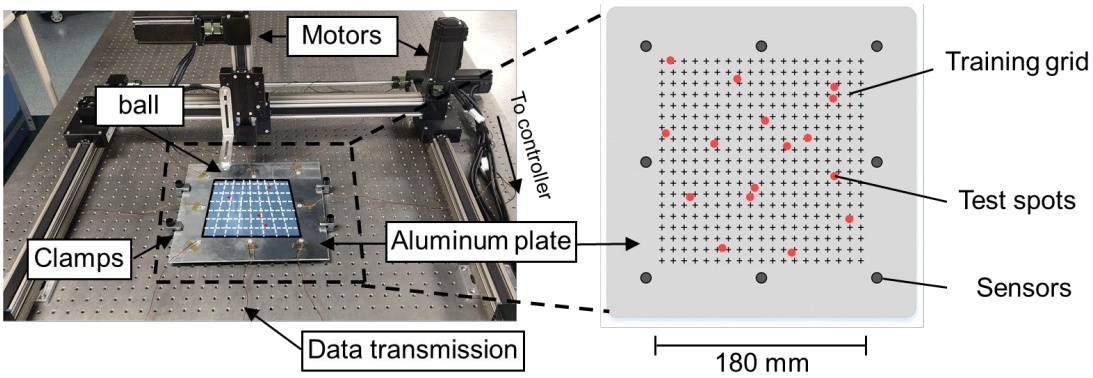

Figure 6. Self-assembled three-axis automated impact stage and arrangement of training and test spots.

The training area is 180×180 mm^2 with a 10 mm grid. To account for the stochastic nature of impact AE signals, three times drop impact were simulated on each spot at each of six different heights (10, 15, 20, 25, 30, 35 mm). Thus, a total number of 6498 sets of pristine training data were obtained with 361 training spots. The random-faulty-channel dataset for training the fail-safe model was achieved by artificially deactivating λ channels. To obtain a generalized model, every possible faulty-channel case needed to be included, *e.g.*, C_8^1 cases for $\lambda = 1$, C_8^2 cases for $\lambda = 2$. Theoretically, λ can be varied from 1 to 7 and one pristine set of original data can be augmented by $C_8^1 + C_8^2 + \cdots + C_8^7 = 254$ times. Although in-turn exhaustively deactivating channels can augment massive data, it will be time-consuming and impractical to train. In this study, for convenience, at least 3 functioned sensors were considered, *i.e.,* λ varied from 1 to 5. For each λ-faulty-channel case, λ random-selected channels were deactivated for every pristine 8-channel impact data. In such a partial augmentation way, the size of the fail-safe training dataset was five times of the pristine

dataset and the generalization purpose for different faulty-channel cases was fulfilled. The test data for the pristine model were generated by drop impact at 16 random-selected spots with six heights, and the total number was 96. The test data for the fail-safe model were obtained in a similar way but with artificially malfunctioned channels.

The dataset for the binary classification was generated by collecting 500 good single-channel signals and 100 bad signals during the experiment as poor clamping, loose connection, and drop directly upon sensors, 450/90 for training and 50/10 for testing. After training 100 epochs, the model can correctly classify the signal with an accuracy of over 98.5%. Such a model needs only 4.16 ms to process a single 8-channel data.

4.2. Results and discussions

To qualify the performance of models, the loss function and accuracy are firstly defined. The AE signals of all eight sensors from *n*-th impact case are paralleled sequentially as the input vector $\boldsymbol{X_n} \in \mathbb{R}^{8\times \mathrm{SPs}}$. In the proposed intersection-clustering method, the corresponding impact location is calculated from its source-sensor distances as the output vector $\boldsymbol{Y_n} \in \mathbb{R}^{1\times 8}$, while for the common "End-to-End" method, the corresponding impact location is directly indicated by its *x* and *y* coordinates as the output vector $\boldsymbol{Y_n} \in \mathbb{R}^{1\times 2}$. In the training phase, the impact locations are known and used to generate labels. The training process is to optimize the parameters in the model to minimize a loss function of mean squared error between the outputs of the model and the labels,

$$\mathrm{Loss} = \left\| \mathsf{F}\left(\{\boldsymbol{X}_n\}\right) - \left\{\hat{\boldsymbol{Y}}_n\right\} \right\|_2^2, \tag{2}$$

where $\{\boldsymbol{X_n}\}$ is the input dataset and $\{\widehat{\boldsymbol{Y}}_{\boldsymbol{n}}\}$ is the label dataset. $\mathcal{F}$ is the mapping function of the proposed 1D-ResNet model.

The predicted accuracy of impact location is defined by normalizing mean localization error (MLE) with respect to the size of the inspected area. MLE is the average distances from the predicted location (x_n, y_n) to the real coordinates of impact source $(\hat{x}_n, \hat{y}_n)$ for N impact cases,

$$\begin{aligned} \text{MLE} &= \frac{\sum_{n=1}^{N}\sqrt{(x_n-\hat{x}_n)^2+(y_n-\hat{y}_n)^2}}{N} \\ \text{Accuracy} &= 1-\frac{\text{MLE}}{D_{Inspected}}\times 100\% \end{aligned}, \quad \textbf{(3)}$$

where $D_{Inspected}$ is the dimension size of the inspected area and is 180 mm in this study.

4.2.1. Influence of window length of input data

In general, the DL model can learn more features with longer input data. However, the training cost, such as computing time and memory, must be considered in reality. The selected window length cannot be too short that fails to provide sufficient features, nor too long that rises computing burden. Thus, input data with different window lengths (of 2048, 3072, 4096, 5120, and 6144 SPs) were trained respectively by the same 1D-ResNet architecture for 200 Epochs with Adam optimizer. The performance of the pristine model was exhibited as Loss and Accuracy curves of training and test datasets (labeled as tr_loss, tr_accuracy, test_loss, test_accuracy, respectively) with respect to epochs in **Figure 7a-e**. The final values of them with other performance parameters were summarized in **Table 2**.

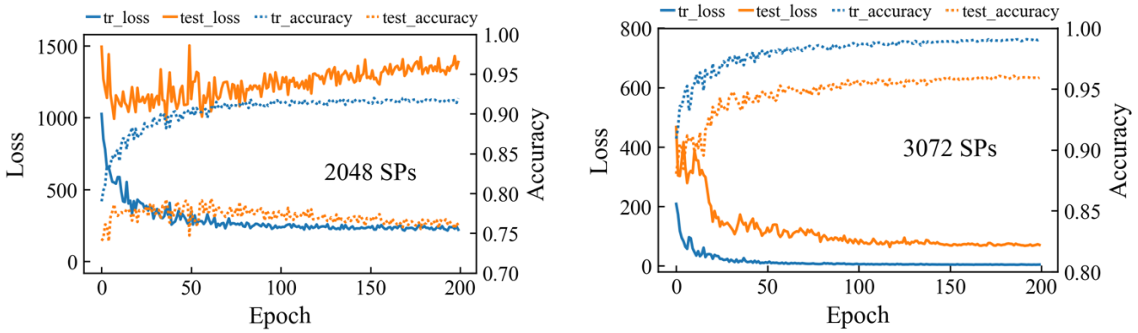

(a) (b)

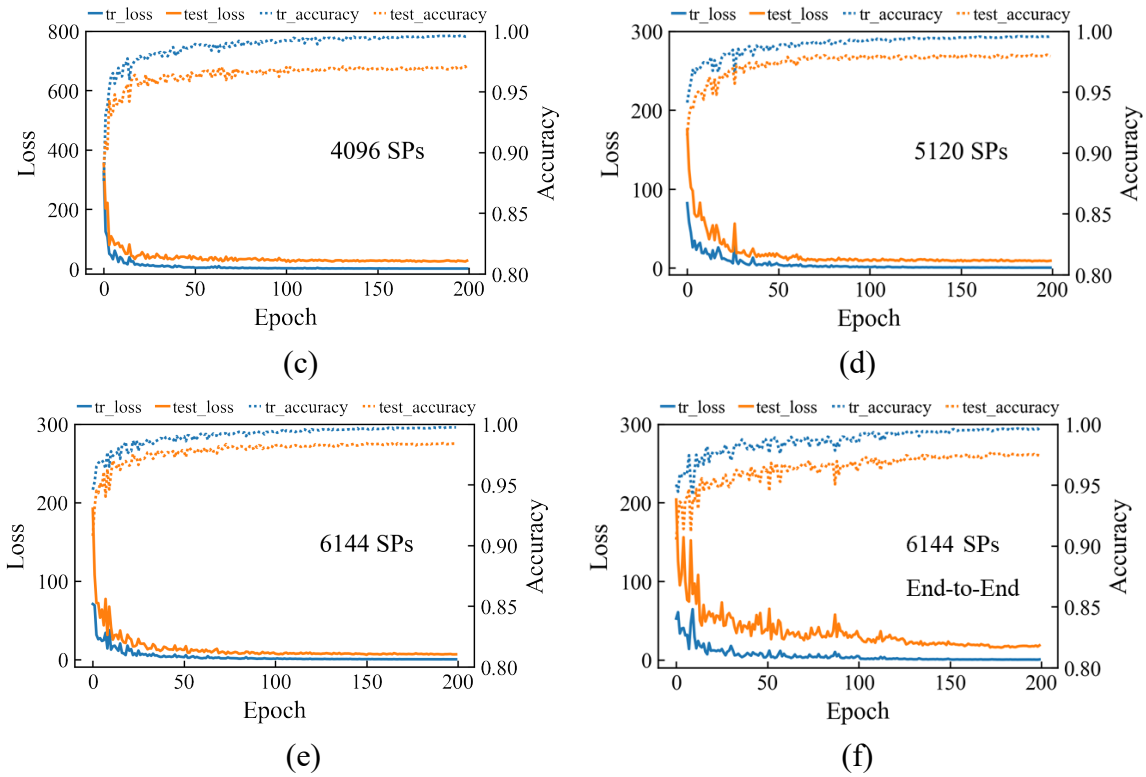

Figure 7. Loss and accuracy curves of the pristine model with different window lengths of input data: (a) 2048 SPs; (b) 3072 SPs; (c) 4096 SPs; (d) 5120 SPs; (e) 6144 SPs; (f) "End-to-End" model with window length of 6144 SPs.

Table 2

Model performance with different window lengths of input data.

Window length	2048	3072	4096	5120	6144
Final tr_loss	222.74	3.60	0.41	0.57	0.22
Final test_loss	1387	70	27	9	6
Final tr_accuracy (%)	91.92	99.06	99.59	99.54	99.71
Final test_accuracy (%)	75.99	95.94	96.86	97.94	98.38
Final accuracy difference (%)	15.93	3.12	2.73	1.6	1.33
Final training MLE (mm)	14.55	1.69	0.73	0.83	0.53
Final test MLE (mm)	43.22	7.31	5.65	3.71	2.91
Time effort per step (ms)	3.57	4.13	4.39	4.72	5.45

With a window length of 2048 SPs, both the loss and accuracy curves exhibit unstable performance with epochs in **Figure 7a**, and the final accuracy difference between training and test data is as large as ~16% (the blue dash line and orange dash line), which indicates a high degree of over-fitting. The model cannot learn sufficient useful features from the short training data and give poor predicted results. When the window length is extended to 3072

SPs and longer, the final test accuracy can reach higher than 95%. Both the loss and accuracy curves show smooth and fast convergence in **Figure 7b-e**. The test accuracy improves gradually with increasing window length as expected. For the longest input window length of 6144 SPs, the final test accuracy can reach as high as ~98%, which is very close to the corresponding final training accuracy.

The required time per training step increases steadily with the increase of window length from 3.57 ms to 5.45 ms. This is also the processing time per impact case in the test phase, which is suitable for real-time SHM. Such short time cost is benefitted from raw signal input without data pre-processing. The training time per epoch can be estimated by further multiplying by the amount of data in the training set, which is 6498. Since the training time is acceptable in our lab environment, 200 epochs and 6144 SPs were used for the following studies. For a more efficient training process in industrial applications, a trade-off between test accuracy and training time must be considered by reducing epochs of training and window length of input data.

4.2.2. Influence of target of output

In this study, the impact location was obtained by the proposed intersection-clustering method with source-to-sensor distance output from the model. To study the influence of forms of output data, a similar model with "End-to-End" output was implemented for comparison. The last layer of the "End-to-End" model outputted directly the coordinates of impact location while the other structures remained the same. The training and test procedures were implemented in the same way and loss and accuracy curves are shown in **Figure 7f**.

Through comparing **Figure 7f** with **Figure 7e**, it is obvious that the proposed model has

better performance than the "End-to-End" model during training. The test accuracy is higher and the difference of accuracy between training and test is smaller. The convergence of both loss and accuracy curves are smoother and faster. The "End-to-End" model, on the other hand, has relatively good performance on the loss and accuracy curves of the training dataset, while poor performance on the loss and accuracy curves of the test dataset, which implies a worse over-fitting issue. It should be noted that the proposed model can achieve stable and accurate results within only 100 epochs, which shows the potential for more efficient training progress. The predicted location error is visualized in **Figure 8** with all test data. The proposed intersection-clustering method can clearly achieve more accurate predicted impact locations. The results indicate that relaxing targets of convergence can help mitigate the over-fitting issue, especially in this study the targets of output as source-to-sensor distances having clear physical meaning.

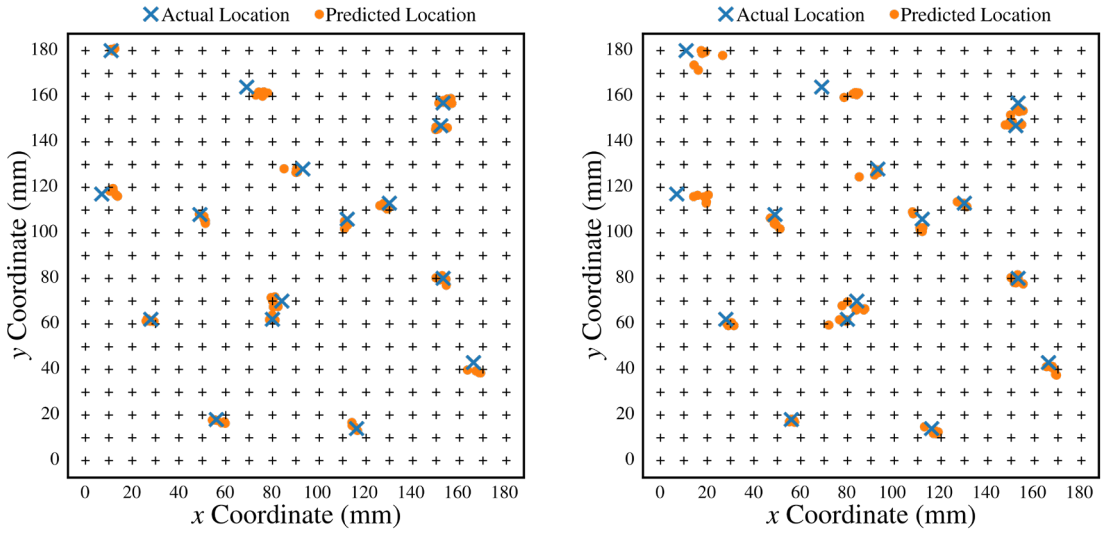

Figure 8. Predicted and actual impact locations: (a) proposed model with intersection-clustering method; (b) "End-to-End" model.

4.2.3. Performance of fail-safe model

To adapt to random faulty-channel situations, the DL model needs to be generalized enough by considering all possible faulty-channel situations. The training dataset is a big problem that it is not possible to generate sufficient and diverse data through experiments. In this

study, a data augmentation technique was implemented. The training dataset for the fail-safe model was generated from the pristine training dataset by artificially zeroing random channels, and the size was 5 times larger. Transfer learning was performed to train the new model for high efficiency and accuracy, with the help of pre-trained parameters from the existing pristine model.

Several cases were discussed in the test phase to validate the proposed fail-safe model. The study cases were divided by the number of random faulty channels as λ-random-faulty-channel (λ-RFC, λ=1, 2, 3, 4, 5) and pristine (0-random-faulty-channel) cases. The fail-safe test data were similarly generated from pristine test data as the training data. For each 8-channel AE signal set from a single impact event at randomly selected test spots, λ sensors were selected randomly and deactivated by zeroing the AE signals of corresponding channels. In such a way, the size of the test dataset for each λ-RFC case was the same as for the pristine case. The training curve and test results of the fail-safe model are shown in **Figure 9**. It can be observed that the training loss curve and all the test accuracy curves show smooth and steady convergence within 200 epochs. When the number of faulty channels increases from 1 to 4, the predicted accuracies only decrease slightly, remaining above 96%, which is comparable to the accuracy of the pristine model for pristine data (98.38%). For the 5-RFC case, the accuracy drops suddenly below 94%. In this situation, only three sensors are functioned and could not contribute enough useful features. It can also be observed from the test localization error distributions in **Figure 10**. When the number of faulty channels is less than 5, the distribution of the location error is bell-shaped and concentrated in the low error area. For 5-RFC, the location error increases and is concentrated in the high error area, Interestingly, when testing pristine data on the fail-safe model, the predicted accuracy is higher than RFC cases (97.59%), although not as good as obtained on the pristine model.

Even the parameters were retrained for fail-safe adaptation, the high generalization performance of the fail-safe model enables it to process pristine data well.

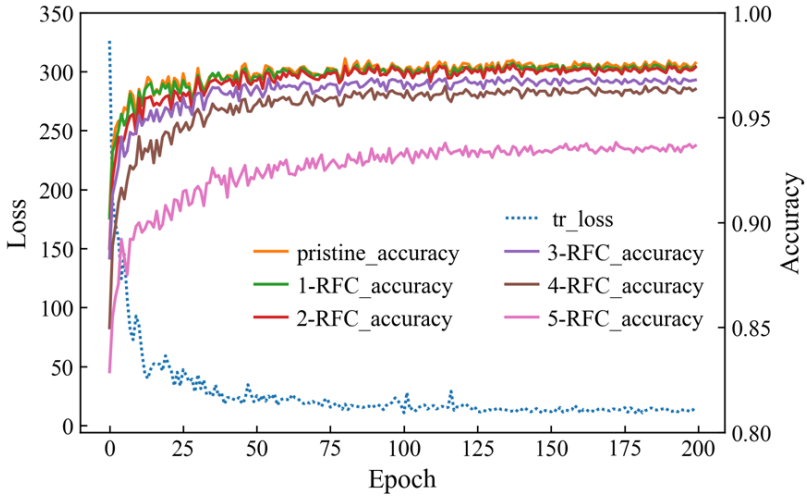

Figure 9. Training curve and test results of fail-safe model.

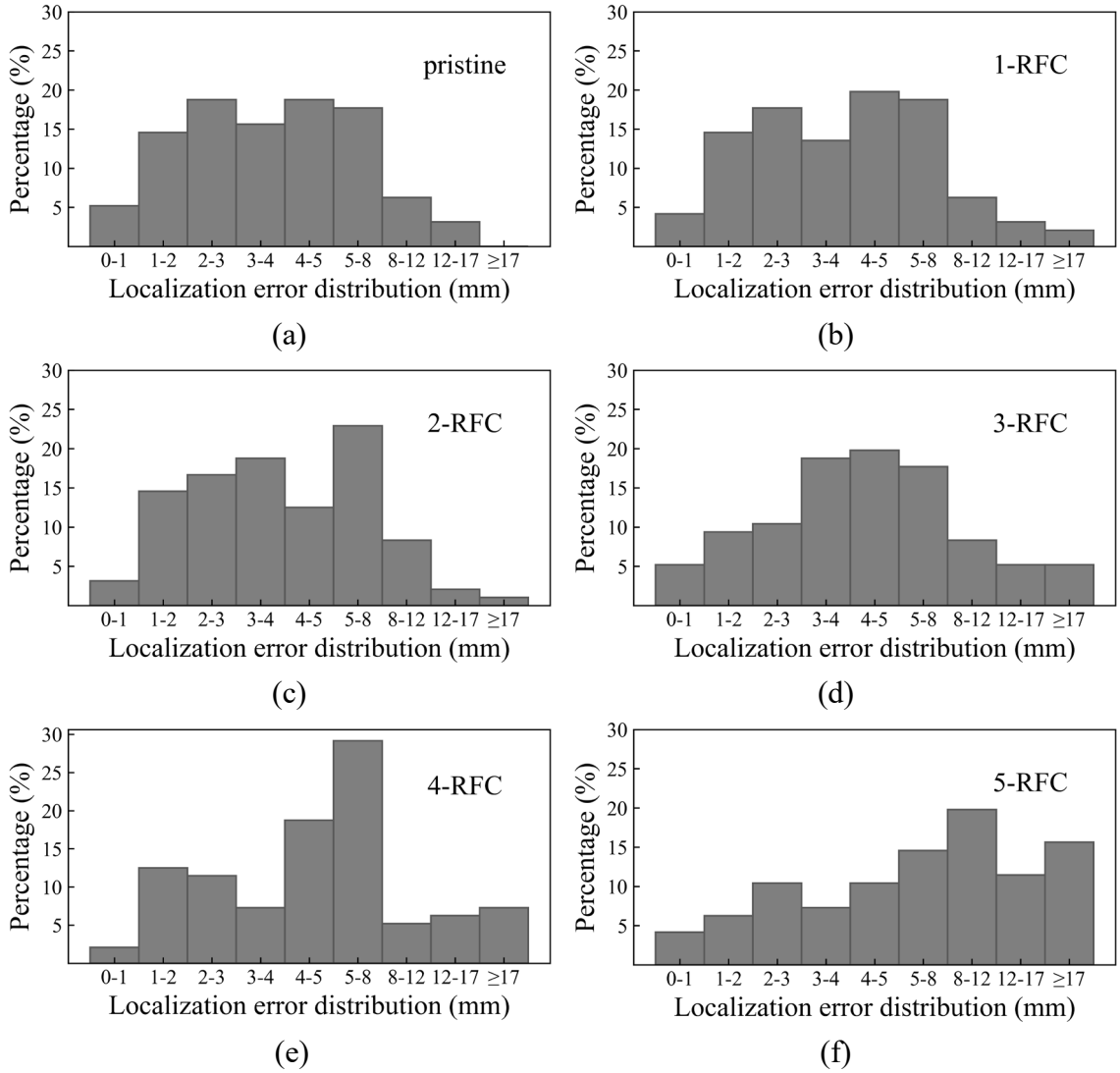

Figure 10. Histograms of localization error distribution of fail-safe model tested by: (a) pristine;

(b) 1-RFC; (c) 2-RFC; (d) 3-RFC; (e) 4-RFC; (f) 5-RFC.

To validate the superiority of the fail-safe model, the same λ-RFC test data were also fed to the pristine model. The final predicted results are summarized in **Table 3**. The pristine model fails to handle random-faulty-channel cases. The accuracy of predicted impact locations decreases dramatically with the number of faulty channels increasing. The location error increases from 2.91 to 48.51 mm with an accuracy of 73.05% for 5-RFC case. In summary, the pristine model has low level of reliability and robustness. On the other hand, the proposed fail-safe model shows good and constant prediction performance under all cases, which exhibits a great potential for in-situ SHM applications in real scenarios. **Figure 11** gives the localization results of the 1-RFC case by the pristine model and fail-safe model, where the difference in predicted accuracy can be seen clearly.

Table 3
Performance of pristine model and fail-safe model under different test cases.

Test case	pristine	1-RFC	2-RFC	3-RFC	4-RFC	5-RFC
Test MLE of pristine model (mm)	2.91	10.24	15.95	25.05	33.31	48.51
Test MLE of fail-safe model (mm)	4.33	4.63	4.69	5.77	6.56	11.41
Test accuracy of pristine model (%)	98.38	94.31	91.14	86.08	81.49	73.05
Test accuracy of fail-safe model (%)	97.59	97.43	97.42	96.79	96.36	93.66

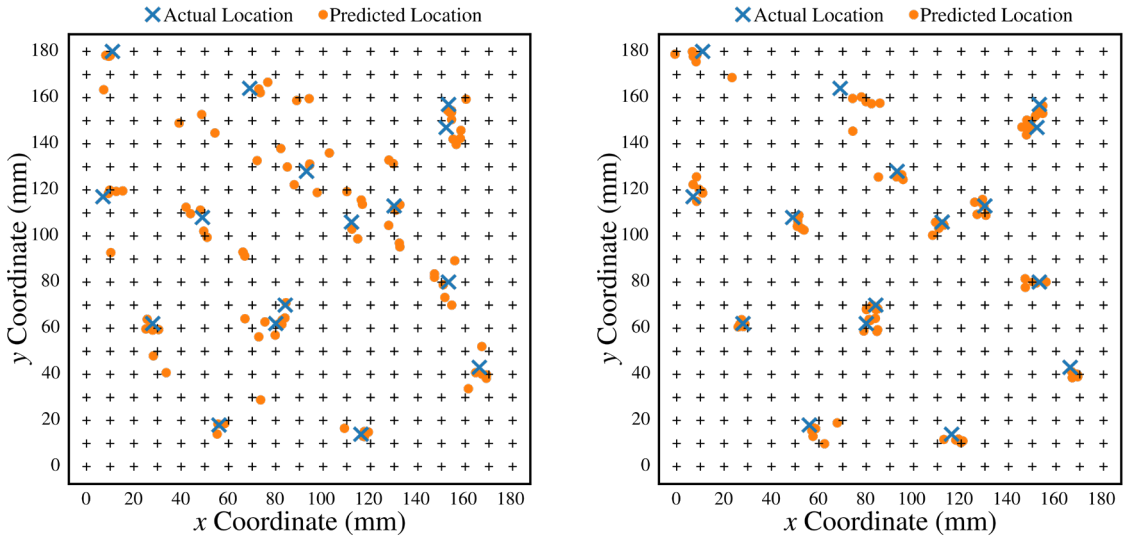

Figure 11. Localization results of 1-RFC: (a) pristine model; (b) fail-safe model.

For various forms of error signals in real scenarios, the whole framework works in the following steps. Firstly, a 1D-CNN classification model was used to process the raw signals. For all-good-channel cases, the pristine model is used to predict. Faulty channels once identified, if any, are uniformed by setting all error signals to zero values, in such a way to conform to the data form in the fail-safe training dataset. Then the fail-safe model is used to predict. To validate the whole framework, 3 sensors at the top left corner were disconnected on purpose when performing impact tests and treated as validation case 1. Validation case 2 was disconnecting 3 sensors at the bottom right corner. Thus, the obtained AE signals in these two cases have three channels of only noise. The localization results are shown in **Figure 12**. Comparing **Figure 12a** and **Figure 8a**, it can be found that poorer results are predicted when the impact source is located near the top left corner. The same phenomenon can be found in **Figure 12b**, where the accuracy of impact at the bottom right corner decrease with 3 malfunctional sensors around. These results are consistent with physical knowledge that the AE signals of nearby sensors can help produce more accurate results of impact locations than faraway sensors, due to dispersion and signal complexity after long-distance Lamb wave propagation. It also proves that the DL model has successfully learned this physical problem and weighted different contributions of sensors to the final predicted results based on source-to-sensor distances.

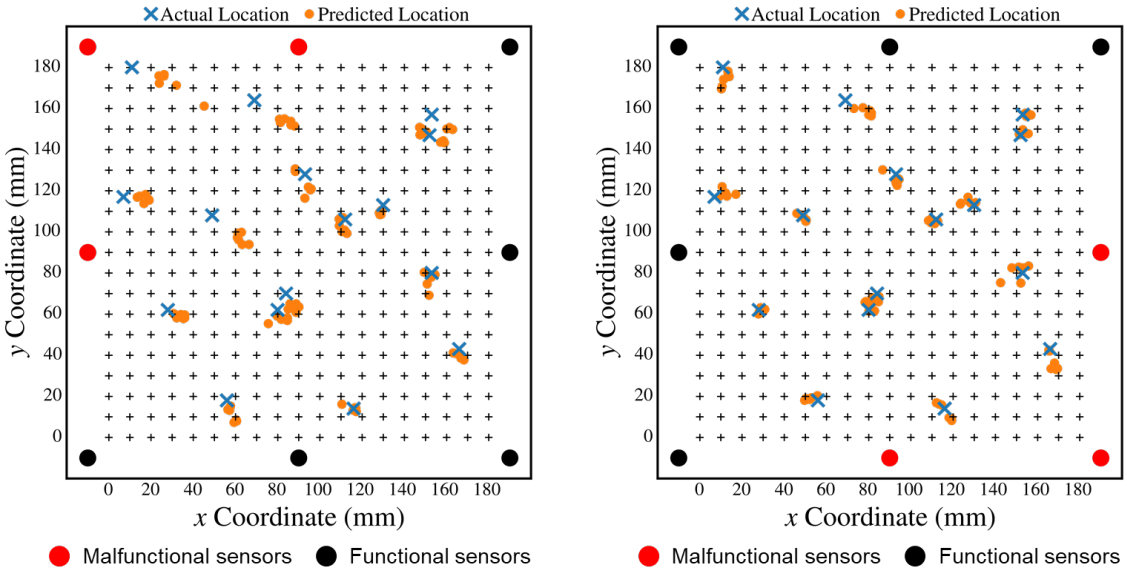

Figure 12. Localization results of fail-safe model: (a) validation case 1; (b) validation case 2.

5. Case Study on A Complex Inhomogeneous Plate

5.1. Experimental setup and dataset acquisition

As shown in **Figure 13**, a larger plate with a size of 500×500 mm^2 and a thickness of 2 mm was chosen with a network of 8 sensors. Two artificial cavities were manufactured on the plate to create inner boundaries which complicated the AE signals from impact location to sensors as in **Figure 2**. The training area is 400×400 mm^2 with a 20 mm grid. Three times of drop impact were simulated on each spot at each of six different heights (10, 15, 20, 25, 30, 35 mm). Thus, a total number of 7434 sets of pristine training data were obtained with 413 training spots (28 spots lost due to cavities). Considering the longer propagation path, the acquisition length was increased to 12288 SPs by trial and error as in **Section 4.2.1**. The other settings were similar to **Section 3.1**.

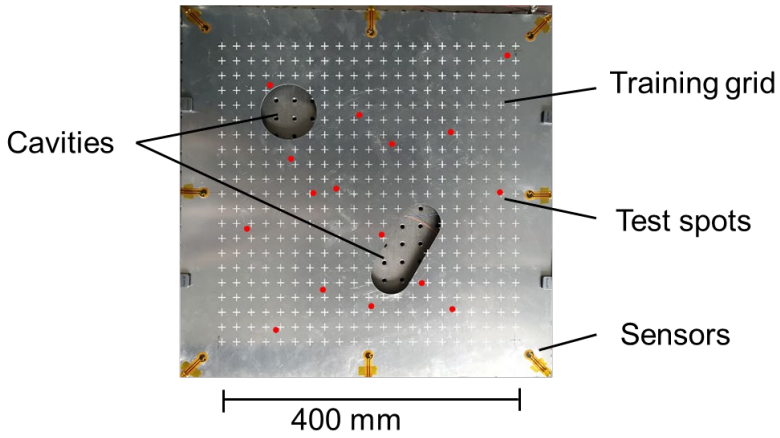

548
549 **Figure 13.** Illustration of the complex inhomogeneous plate and arrangement of training and test
550 spots.

551 *5.2. Results and discussions*

552 The proposed model with the intersection-clustering method was firstly performed under
553 pristine conditions. Similarly, the results were compared with the "End-to-End" model. Loss
554 and accuracy curves are shown in **Figure 14**. The proposed model outperforms again with a
555 complex inhomogeneous plate. The test accuracy is higher and the difference in accuracy
556 between training and test is smaller. The convergence of both loss and accuracy curves are
557 smoother and faster. The predicted location error is visualized in **Figure 15** with all test data.
558 The results are consistent with those of a simple homogeneous plate and verify the
559 effectiveness of the proposed method to improve the accuracy of predicted impact locations.
560 Although with more complicated AE signals, the DL model can successfully learn features
561 for impact localization at a high-level accuracy, which is comparable with the result of a
562 simple plate. The test MLE is 7.33, which is larger than the 2.91 of the simple plate, but the
563 test accuracy is close, 98.17% *vs* 98.38%, due to the larger inspected area.

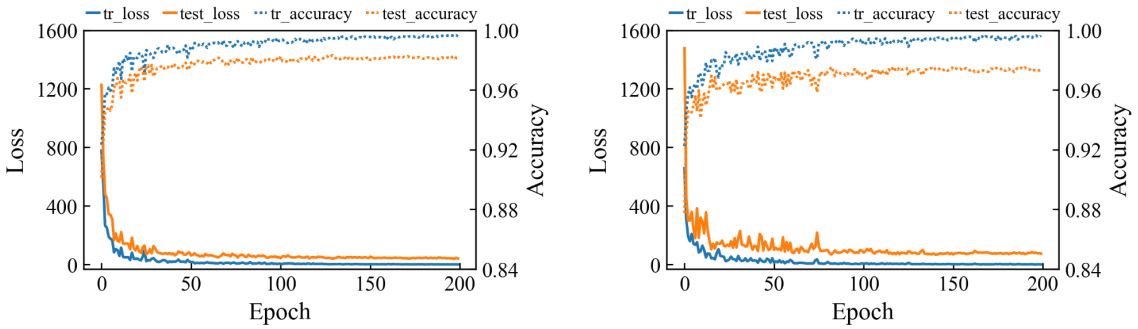

Figure 14. Loss and accuracy curves of (a) proposed pristine model with intersection-clustering method; (b) "End-to-End" model.

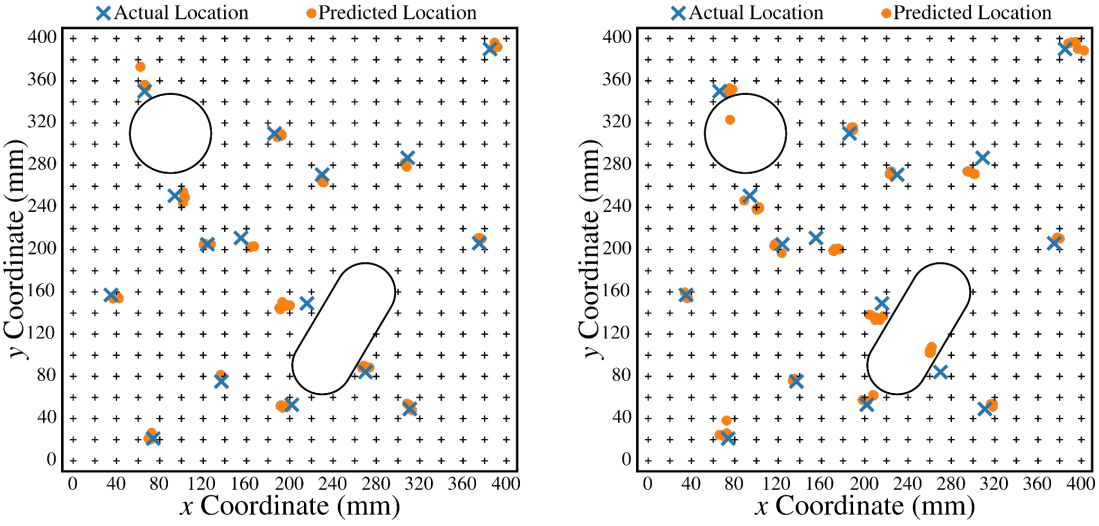

Figure 15. Predicted and actual impact locations: (a) proposed model with intersection-clustering method; (b) "End-to-End" model.

The performance of the fail-safe model was also verified with the complex plate. The final predicted results are summarized in **Table 4**. The results are also consistent with the previous one with a simple plate. The accuracy of predicted impact locations decreases dramatically for the pristine model with the number of faulty channels increasing. For the fail-safe model, the location accuracy only decreases slightly to 95.10% for the 5-RFC case, compared to 75.75% of the pristine model. The proposed fail-safe model can achieve relatively stable accurate prediction of impact locations under diverse random-faulty-channel cases, which has proven to be reliable and robust enough for practices in complex SHM applications.

Table 4
Performance of pristine model and fail-safe model under different test cases.

Test case	pristine	1-RFC	2-RFC	3-RFC	4-RFC	5-RFC
Test MLE of pristine model (mm)	7.33	25.05	32.64	46.41	70.32	96.99
Test MLE of fail-safe model (mm)	7.61	8.18	8.26	8.93	11.97	19.61
Test accuracy of pristine model (%)	98.17	93.74	91.84	88.40	82.42	75.75
Test accuracy of fail-safe model (%)	98.10	97.96	97.94	97.77	97.01	95.10

582

583 **6. Concluding Remarks**

584 In this study, a hierarchical deep convolutional regression framework with fail-safe
585 adaptation is proposed for impact localization from AE signals. A multi-branch 1D-ResNet
586 model was used to process raw time-series data for feature extraction, followed by a
587 regression layer to obtain source location results. The pristine model was trained by a full-
588 functioned-channel dataset. The fail-safe adaptation was achieved by transferring the pristine
589 model to learn from a random-faulty-channel dataset, which was augmented from the full-
590 functioned-channel dataset. To implement such framework, signal data from each channel
591 was first binary classified by a simple 1D-CNN model for further processing by either
592 pristine or fail-safe model. The regressive output was source-to-sensor distances. The final
593 predicted impact location was obtained by a proposed intersection-clustering method.
594 Without the need for signal pre-processing, the whole process takes only a few milliseconds
595 for a single impact case (4.16+5.45 ms), which is well suited for real-time SHM.

596

597 The performance of the well-trained model was qualified by loss and location accuracy. By
598 comparing different window lengths of input data, it can be concluded that the balance
599 between accuracy and training speed can be achieved when using a proper window length
600 containing sufficient features. The performance of outputting source-to-sensor distances
601 with the proposed intersection-clustering method is better than that of outputting merely
602 location coordinates with the “End-to-End” model. Such quality control of input and output

603 would achieve a certain degree of physical bias, leading to the mitigated over-fitting status.
604 These results show that high-level accuracy has been achieved with the raw time-series
605 signals, which contain sufficient features for 1D-CNN models to learn from. In other cases,
606 where insufficient features are available, *e.g.* with few sensors or a large inspected area,
607 including frequency or time-frequency domain information could be a possible way to
608 increase the prediction accuracy.
609
610 Although the well-trained pristine model can predict accurate impact location in normal
611 situations with all sensors fully functioned, it is not general enough to handle abnormal
612 situations with faulty channels, which is complicated and not rare in *in-situ* SHM
613 applications with fixed sensor networks. The fail-safe model has a much better performance
614 than the pristine model when handling random-faulty-channel cases. The predicted location
615 error could maintain at a low level with even five faulty channels, which is about 10 mm
616 compared to ~50 mm error predicted by the pristine model. Thus, the proposed framework
617 has proven to be effective for various faulty scenarios of the sensor network during operation
618 of the inspected structure, and exhibits a high level of reliability and robustness as a DL-
619 assisted automated *in-situ* SHM method. These results were further validated on a complex
620 structure. More complicated AE signals were obtained due to inhomogeneous features which
621 were extremely difficult to process with physics-based methods. The proposed DL method
622 has achieved high-level accuracy of impact localization again with fail-safe adaptation.
623
624 This work may not be the ultimate answer to using DL for SHM. However, it provides a
625 solution to solve a practical issue that is common in reality but seldomly considered in the
626 lab environment. The sensor network fail-safe adaptation realized by data augmentation and
627 transfer learning can be extended to other SHM methods including active Lamb wave-based

technology without additional experiments. Generalizing DL models makes a step further to bridge lab experiments and practical industry applications with much more variables, and gains trust in DL algorithms by relieving worries about insufficient and imbalanced training data. It should be mentioned that, a side benefit is implied that the fail-safe model should also work well for sensor network deployments with fewer sensors such as a four-corner sensor network, without the need for retraining.

CRediT authorship contribution statement

Shifeng Guo: Project administration, Supervision, Resources, Writing - review & editing, Funding acquisition. **Hao Ding**: Investigation, Data curation, Formal analysis, Visualization, Writing - original draft. **Yehai Li**: Conceptualization, Methodology, Validation, Writing - original draft, Writing - review & editing. **Haowen Feng**: Investigation, Data curation, Formal analysis. **Xinhong Xiong**: Supervision, Writing - review & editing. **Zhongqing Su**: Validation, Writing - review & editing. **Wei Feng**: Project administration, Supervision, Writing - review & editing.

Declaration of Competing Interest

The authors declare that they have no known competing financial interests or personal relationships that could have appeared to influence the work reported in this paper.

Acknowledgments

This project is supported in part by the National Natural Science Foundation of China (Grant Nos. 52005493, U2133213, 52071332, and U1813222), in part by the Department of Science and Technology of Guangdong Province (Grant Nos. 2019QN01H430 and 2019TQ05Z654), and in part by the Science and Technology Innovation Commission of Shenzhen (Grant No.

651 ZDSYS20190902093209795, JCYJ20180507182239617, and JCYJ20210324101200002).

652 **References**

653 [1] V. Giurgiutiu, Structural Health Monitoring with Piezoelectric Wafer Active Sensors, 2nd ed.,
654 Academic Press, 2014.
655 [2] Y. Li, K. Wang, W. Feng, H. Wu, Z. Su, S. Guo, Insight into excitation and acquisition mechanism
656 and mode control of Lamb waves with piezopolymer coating-based array transducers: Analytical and
657 experimental analysis, Mech. Syst. Signal Pr., 178 (2022) 109330.
658 https://doi.org/10.1016/j.ymssp.2022.109330
659 [3] C. Zhang, Z. Zhang, H. Ji, J. Qiu, C. Tao, Mode conversion behavior of guided wave in glass
660 fiber reinforced polymer with fatigue damage accumulation, Compos. Sci. Technol. , 192 (2020)
661 108073. https://doi.org/10.1016/j.compscitech.2020.108073
662 [4] Z. Su, L. Ye, Identification of damage using Lamb waves: from fundamentals to applications,
663 Springer Science & Business Media, 2009.
664 [5] K. Xu, D. Ta, Z. Su, W. Wang, Transmission analysis of ultrasonic Lamb mode conversion in a
665 plate with partial-thickness notch, Ultrasonics, 54 (2014) 395-401.
666 https://doi.org/10.1016/j.ultras.2013.07.011
667 [6] C. Zhang, Y. Huang, C. Tao, J. Qiu, H. Ji, Fatigue property evaluation for fiber reinforced plastics
668 based on mode conversion effect of guided wave, Compos. Sci. Technol. , 223 (2022) 109405.
669 https://doi.org/10.1016/j.compscitech.2022.109405
670 [7] F.-G. Yuan, S.A. Zargar, Q. Chen, S. Wang, Machine learning for structural health monitoring:
671 challenges and opportunities, SPIE Smart Structures + Nondestructive Evaluation, Proc. SPIE 11379,
672 2020. https://doi.org/10.1117/12.2561610
673 [8] Y. Bao, H. Li, Machine learning paradigm for structural health monitoring, Struct. Health Monit.,
674 20 (2020) 1353-1372. https://doi.org/10.1177/1475921720972416
675 [9] X. Wang, G. Foliente, Z. Su, L. Ye, Multilevel Decision Fusion in a Distributed Active Sensor
676 Network for Structural Damage Detection, Struct. Health Monit., 5 (2006) 45-58.
677 https://doi.org/10.1177/1475921706057981
678 [10] Y. Ying, H. Garrett James, J. Oppenheim Irving, L. Soibelman, B. Harley Joel, J. Shi, Y. Jin,
679 Toward Data-Driven Structural Health Monitoring: Application of Machine Learning and Signal
680 Processing to Damage Detection, J. Comput. Civil. Eng., 27 (2013) 667-680.
681 https://doi.org/10.1061/(ASCE)CP.1943-5487.0000258
682 [11] Z. Su, L. Ye, Lamb wave-based quantitative identification of delamination in CF/EP composite
683 structures using artificial neural algorithm, Compos. Struct., 66 (2004) 627-637.
684 https://doi.org/10.1016/j.compstruct.2004.05.011
685 [12] J.R. LeClerc, K. Worden, W.J. Staszewski, J. Haywood, Impact detection in an aircraft

composite panel—A neural-network approach, J Sound Vib, 299 (2007) 672-682. https://doi.org/10.1016/j.jsv.2006.07.019
[13] J. Haywood, P.T. Coverley, W.J. Staszewski, K. Worden, An automatic impact monitor for a composite panel employing smart sensor technology, Smart Mater. Struct., 14 (2004) 265-271. https://doi.org/10.1088/0964-1726/14/1/027
[14] S. Khan, T. Yairi, A review on the application of deep learning in system health management, Mech. Syst. Signal Pr., 107 (2018) 241-265. https://doi.org/10.1016/j.ymssp.2017.11.024
[15] Y.-J. Cha, W. Choi, O. Büyüköztürk, Deep Learning-Based Crack Damage Detection Using Convolutional Neural Networks, Computer-Aided Civil and Infrastructure Engineering, 32 (2017) 361-378. https://doi.org/10.1111/mice.12263
[16] W. Hou, Y. Wei, J. Guo, Y. Jin, C.a. Zhu, Automatic Detection of Welding Defects using Deep Neural Network, J. Phys: Conf. Ser., 933 (2018) 012006. https://doi.org/10.1088/1742-6596/933/1/012006
[17] L. Ruan, B. Gao, S. Wu, W.L. Woo, DeftectNet: Joint loss structured deep adversarial network for thermography defect detecting system, Neurocomputing, 417 (2020) 441-457. https://doi.org/10.1016/j.neucom.2020.07.093
[18] C. Tao, C. Zhang, H. Ji, J. Qiu, Fatigue damage characterization for composite laminates using deep learning and laser ultrasonic, Composites Part B: Engineering, 216 (2021) 108816. https://doi.org/10.1016/j.compositesb.2021.108816
[19] T. Kundu, Acoustic source localization, Ultrasonics, 54 (2014) 25-38. https://doi.org/10.1016/j.ultras.2013.06.009
[20] S.K. Al-Jumaili, M.R. Pearson, K.M. Holford, M.J. Eaton, R. Pullin, Acoustic emission source location in complex structures using full automatic delta T mapping technique, Mech. Syst. Signal Pr., 72-73 (2016) 513-524. https://doi.org/10.1016/j.ymssp.2015.11.026
[21] F. Ciampa, M. Meo, Acoustic emission localization in complex dissipative anisotropic structures using a one-channel reciprocal time reversal method, The Journal of the Acoustical Society of America, 130 (2011) 168-175. https://doi.org/10.1121/1.3598458
[22] C. Chen, F.-G. Yuan, Impact source identification in finite isotropic plates using a time-reversal method: theoretical study, Smart Mater. Struct., 19 (2010) 105028. https://doi.org/10.1088/0964-1726/19/10/105028
[23] A. Ebrahimkhanlou, S. Salamone, Acoustic emission source localization in thin metallic plates: A single-sensor approach based on multimodal edge reflections, Ultrasonics, 78 (2017) 134-145. https://doi.org/10.1016/j.ultras.2017.03.006
[24] R. Ernst, F. Zwimpfer, J. Dual, One sensor acoustic emission localization in plates, Ultrasonics, 64 (2016) 139-150. https://doi.org/10.1016/j.ultras.2015.08.010
[25] A. Ebrahimkhanlou, S. Salamone, Single-sensor acoustic emission source localization in plate-like structures: a deep learning approach, SPIE Smart Structures and Materials + Nondestructive

723 Evaluation and Health Monitoring, Proc. SPIE 10600, 2018. https://doi.org/10.1117/12.2296613
724 [26] A. Ebrahimkhanlou, B. Dubuc, S. Salamone, A generalizable deep learning framework for
725 localizing and characterizing acoustic emission sources in riveted metallic panels, Mech. Syst. Signal
726 Pr., 130 (2019) 248-272. https://doi.org/10.1016/j.ymssp.2019.04.050
727 [27] D.F. Hesser, S. Mostafavi, G.K. Kocur, B. Markert, Identification of acoustic emission sources
728 for structural health monitoring applications based on convolutional neural networks and deep
729 transfer learning, Neurocomputing, 453 (2021) 1-12. https://doi.org/10.1016/j.neucom.2021.04.108
730 [28] S.A. Zargar, F.-G. Yuan, Impact diagnosis in stiffened structural panels using a deep learning
731 approach, Struct. Health Monit., 20 (2020) 681-691. https://doi.org/10.1177/1475921720925044
732 [29] H. Liu, Y. Zhang, Deep learning based crack damage detection technique for thin plate structures
733 using guided lamb wave signals, Smart Mater. Struct., 29 (2019) 015032.
734 https://doi.org/10.1088/1361-665x/ab58d6
735 [30] V. Ewald, R. Sridaran Venkat, A. Asokkumar, R. Benedictus, C. Boller, R.M. Groves, Perception
736 modelling by invariant representation of deep learning for automated structural diagnostic in aircraft
737 maintenance: A study case using DeepSHM, Mech. Syst. Signal Pr., (2021) 108153.
738 https://doi.org/10.1016/j.ymssp.2021.108153
739 [31] P. Pandey, A. Rai, M. Mitra, Explainable 1-D convolutional neural network for damage detection
740 using Lamb wave, Mech. Syst. Signal Pr., 164 (2022) 108220.
741 https://doi.org/10.1016/j.ymssp.2021.108220
742 [32] A. Rai, M. Mitra, Lamb wave based damage detection in metallic plates using multi-headed 1-
743 dimensional convolutional neural network, Smart Mater. Struct., 30 (2021) 035010.
744 https://doi.org/10.1088/1361-665x/abdd00
745 [33] V. Ewald, R.M. Groves, R. Benedictus, DeepSHM: a deep learning approach for structural
746 health monitoring based on guided Lamb wave technique, SPIE Smart Structures + Nondestructive
747 Evaluation, Proc. SPIE 10970, 2019. https://doi.org/10.1117/12.2506794
748 [34] I. Tabian, H. Fu, Z. Sharif Khodaei, A Convolutional Neural Network for Impact Detection and
749 Characterization of Complex Composite Structures, Sensors, 19 (2019).
750 https://doi.org/10.3390/s19224933
751 [35] P. Gardner, X. Liu, K. Worden, On the application of domain adaptation in structural health
752 monitoring, Mech. Syst. Signal Pr., 138 (2020) 106550.
753 https://doi.org/10.1016/j.ymssp.2019.106550
754 [36] Y. Li, W. Feng, L. Meng, K.M. Tse, Z. Li, L. Huang, Z. Su, S. Guo, Investigation on in-situ
755 sprayed, annealed and corona poled PVDF-TrFE coatings for guided wave-based structural health
756 monitoring: From crystallization to piezoelectricity, Materials & Design, 199 (2021) 109415.
757 https://doi.org/10.1016/j.matdes.2020.109415
758 [37] Z.H. Liu, Q.L. Peng, X. Li, C.F. He, B. Wu, Acoustic Emission Source Localization with
759 Generalized Regression Neural Network Based on Time Difference Mapping Method, Exp. Mech.,

60 (2020) 679-694. https://doi.org/10.1007/s11340-020-00591-8
[38] S. Zhang, C.M. Li, W. Ye, Damage localization in plate-like structures using time-varying feature and one-dimensional convolutional neural network, Mech. Syst. Signal Pr., 147 (2021) 107107. https://doi.org/10.1016/j.ymssp.2020.107107
[39] C. Su, M. Jiang, S. Lv, S. Lu, L. Zhang, F. Zhang, Q. Sui, Improved Damage Localization and Quantification of CFRP Using Lamb Waves and Convolution Neural Network, IEEE Sensors Journal, 19 (2019) 5784-5791. https://doi.org/10.1109/JSEN.2019.2908838
[40] F. Ciampa, M. Meo, Acoustic emission source localization and velocity determination of the fundamental mode A0 using wavelet analysis and a Newton-based optimization technique, Smart Mater. Struct., 19 (2010) 045027. https://doi.org/10.1088/0964-1726/19/4/045027
[41] K. Ono, Review on Structural Health Evaluation with Acoustic Emission, 8 (2018) 958. https://doi.org/10.3390/app8060958
[42] L. Capineri, A. Bulletti, Ultrasonic Guided-Waves Sensors and Integrated Structural Health Monitoring Systems for Impact Detection and Localization: A Review, Sensors (Basel), 21 (2021) 2929. https://doi.org/10.3390/s21092929
[43] S. Ji, W. Xu, M. Yang, K. Yu, 3D Convolutional Neural Networks for Human Action Recognition, IEEE Trans. Pattern Anal. Mach. Intell. , 35 (2013) 221-231. https://doi.org/10.1109/TPAMI.2012.59
[44] J. Wu, X. Xu, C. Liu, C. Deng, X. Shao, Lamb wave-based damage detection of composite structures using deep convolutional neural network and continuous wavelet transform, Compos. Struct., 276 (2021) 114590. https://doi.org/10.1016/j.compstruct.2021.114590
[45] S. Sikdar, D. Liu, A. Kundu, Acoustic emission data based deep learning approach for classification and detection of damage-sources in a composite panel, Composites Part B: Engineering, 228 (2022) 109450. https://doi.org/10.1016/j.compositesb.2021.109450
[46] Y. Li, K. Wang, Q. Wang, J. Yang, P. Zhou, Y. Su, S. Guo, Z. Su, Acousto-ultrasonics-based health monitoring for nano-engineered composites using a dispersive graphene-networked sensing system, Struct. Health Monit., (2020) 1475921720929749. https://doi.org/10.1177/1475921720929749
[47] S. Guo, H. Feng, W. Feng, G. Lv, D. Chen, Y. Liu, X. Wu, Automatic Quantification of Subsurface Defects by Analyzing Laser Ultrasonic Signals Using Convolutional Neural Networks and Wavelet Transform, IEEE Trans. Ultrason. Ferroelectr. Freq. Control, 68 (2021) 3216-3225. https://doi.org/10.1109/TUFFC.2021.3087949
[48] A.A. Ijjeh, S. Ullah, P. Kudela, Full wavefield processing by using FCN for delamination detection, Mech. Syst. Signal Pr., 153 (2021) 107537. https://doi.org/10.1016/j.ymssp.2020.107537
[49] K. He, X. Zhang, S. Ren, J. Sun, Deep residual learning for image recognition, Proceedings of the IEEE conference on computer vision and pattern recognition, 2016, pp. 770-778. https://doi.org/10.1109/CVPR.2016.90